Shell-model molecular dynamics calculations of modified silicate glasses

Antonio Tilocca,[1,*] Nora H. de Leeuw,[1,2] and Alastair N. Cormack[1,3]
[1]*Department of Chemistry, University College London, London WC1H 0AJ, United Kingdom*
[2]*School of Crystallography, Birkbeck College, London WC1E 7HX, United Kingdom*
[3]*New York State College of Ceramics, Alfred University, Alfred, New York 14802, USA*
(Received 24 October 2005; revised manuscript received 20 January 2006; published 30 March 2006)

Molecular dynamics simulations of pure silica, sodium silicate, and soda-lime silicate glasses have been carried out using a developed potential that includes polarization effects through the shell model (SM). The potential has been validated using available experimental and *ab initio* structural data, such as density, radial and angular distributions, coordination environments, and network connectivity. In addition, Car-Parrinello molecular dynamics simulations of the soda-lime silicate glass have been carried out to obtain reference data for this system. The performances of the SM and of a rigid-ion potential have been compared with experimental and *ab initio* data, showing that the inclusion of polarization effects improves the description of the intertetrahedral structure and of the local environment surrounding modifier Na and Ca cations; significant improvements are also obtained in the Q^n distribution of the sodium silicate glass. This shows that the inclusion of polarization effects in the potential, even at the approximate level of the shell model, is essential for a reliable modeling of modified bulk glasses. Moreover, the accurate reproduction of the glass density and the direct representation of polarization effects are important requisites that should enable the application of the potential to molecular dynamics simulations of modified glass surfaces.

DOI: 10.1103/PhysRevB.73.104209 PACS number(s): 61.43.Fs, 61.43.Bn

I. INTRODUCTION

Silicate glasses modified with the addition of sodium and calcium oxide have important commercial applications, for example as bioactive materials in medical applications.[1] Advanced experimental techniques,[2–6] such as neutron diffraction, nuclear magnetic resonance (NMR), x-ray absorption fine structure (XAFS), infrared and Raman spectroscopy, as well as computer simulations[7–14] have provided detailed information on the structure of pure silica and sodium silicate glasses, although some aspects of the latter compounds are still controversial, especially concerning the medium-range structure. On the other hand, not as many studies have concerned soda-lime-silicate glasses, probably due to their more complex nature. The structure of pure silica glasses is built up of corner-sharing SiO_4 tetrahedra, where bridging oxygens (BO) link two adjacent Si atoms. In modified silicate glasses, the modifier cations depolymerize the extended network of SiO_4 tetrahedra, breaking Si-O-Si links and forming nonbridging oxygens (NBO) bonded to only one silicon atom. The structure of the modified glasses is then determined by the balance of several interactions, involving partially covalent Si-BO and Si-NBO bonds plus van der Waals and electrostatic forces between the ions. Classical molecular dynamics (MD) simulations have been successfully used to model binary silicate glasses,[7,9,11] but it is hard to obtain an accurate description of complex multicomponent systems, such as soda-lime-silicate glasses, using standard interatomic potentials. In principle, an essential ingredient of a reliable empirical potential for these systems should be the large polarizability of oxygen ions: this factor should be explicitly taken into account in order to model with good accuracy the diverse chemical environments and interactions present in the glasses, such as the peculiar mixture of covalent and ionic contributions in the Si-O bonds. In general, the inclusion of polarization effects, especially for systems with polarizable anions, can improve structural and dynamical properties,[15] and the representation of defects and varying coordination geometries[16–19] is also improved: this feature of the potential is essential to model the glass surfaces and the processes occurring there, such as dissolution and growth processes, which play a key role, for example, in medical applications.[1]

Ideally, the best computational approach would involve *ab initio* MD simulations, for example Car-Parrinello[20] molecular dynamics (CPMD), where the ionic forces are calculated *on the fly* during the simulation from an accurate treatment of the electronic structure using density functional theory: thus many-body and polarization effects are explicitly accounted for. However, even with the large computational resources available today, the size and time scales which can be probed by CPMD are usually around 100–200 atoms and 10–50 ps. Within these limits, recent CPMD simulations[21–25] have provided very accurate data on the local structure and electronic properties of silicate glasses, but in order to probe longer time scales and examine the structure in and beyond the medium range, classical MD is still the only available approach, provided that a reliable potential can be developed. CPMD simulations are nonetheless very useful in this context, as they provide *ab initio* data on the (short-range) local structure of glasses, which are difficult to obtain experimentally, to help the development and assessment of new empirical potentials.

In the polarizable-ion model (PIM) developed by Wilson and Madden,[26] polarization effects in classical MD simulations of ionic systems are accurately represented by the inclusion of ion dipoles as additional degrees of freedom in an extended Lagrangian, and the simultaneous propagation of these additional variables together with the ionic positions is analogous to the Car-Parrinello method. The PIM approach

TABLE I. Shell-model parameters.

	Buckingham potential			
	A (eV)	ρ (Å)	C (eV Å^6)	
O_s-O_s	22764.30	0.14900	27.88	
Si-O_s	1283.91	0.320520	10.661580	
Na-O_s	56465.3453	0.193931	0.0	
Ca-O_s	2152.3566	0.309227	0.099440	
	Three-body harmonic potential			
	k_{3b} (eV rad^{-2})	θ_0 (deg)	ρ (Å)	r_{max} (Å)
O_s-Si-O_s				
Raw (SM0)	2.097	109.47		1.9
Screened (SM1)	100.0	109.47	1.0	2.5
	Core-shell harmonic potential			
	k_{cs} (eV Å^{-2})		Y (e)	
O_c-O_s	74.92		−2.8482	

was successfully applied to the simulation of bulk and surface properties of amorphous SiO_2,[27,28] but no application to multicomponent glasses has been reported. Another simple and consistent way to go beyond rigid-ion models and approximately include polarization effects in an empirical potential is by the shell model of Dick and Overhauser,[29] which can be efficiently implemented in classical MD simulations.[30] Although SM potentials have often been applied to model crystalline oxide materials, including SiO_2,[31–34] no previous application to glasses has been reported. The more rigorous description of ionic polarization in the PIM method makes it in principle more generally applicable compared to the shell model; the main advantage of a shell-model approach in the specific subject examined in the present work is the relatively small effort needed to obtain and include the additional interactions present in multicomponent glasses, allowing a straightforward application of an established shell-model potential for SiO_2 (see below).

In this paper, we describe the development of a shell-model potential for modified Na/Ca silicate glasses, and its application to MD simulations of pure silica, sodium silicate, and soda-lime-silicate glasses. An extensive comparison is made with experimental results and data from CPMD simulations; we have performed CPMD simulations on the soda-lime silicate glass, which complement existing CPMD results on the pure silica and sodium silicate glasses. In addition, the direct comparison with structural data obtained from a rigid-ion potential allows us to assess the effects of the approximate inclusion of polarization through the shell model.

TABLE II. Optimized cell parameters for $Na_2Ca(SiO_3)_2$ and $Na_2Ca_2(SiO_3)_3$; experimental values are shown in parentheses.

	a (Å)	c (Å)	γ
$Na_2Ca(SiO_3)_2$	10.487 (10.500)	13.172 (13.184)	120°
$Na_2Ca_2(SiO_3)_3$	10.514 (10.464)	13.149 (13.176)	120°

II. COMPUTATIONAL DETAILS

A. Classical molecular dynamics simulations

The force field developed in this work is based on the interatomic potential derived by Sanders *et al.* for quartz,[34] which employs full ionic charges. The polarizability of the oxygen ions is incorporated through the shell model:[29] the total charge Z of the ion is split between a core (of charge Z-Y) and a shell (of charge Y), which are coupled by a harmonic spring k_{cs},

$$E_{cs}(r) = \frac{1}{2}k_{cs}r^2. \quad (1)$$

Short-range forces only act on the shells, whereas Coulomb forces act on both shells and cores. The shells are then polarized by the field of the surrounding ions and in this way the local environment of each ion affects its charge distribution: with the further inclusion of three-body interactions (see below), partial covalence effects are approximately accounted for.

MD simulations were carried out with the DL_POLY code,[35] in which the core-shell dynamics is controlled by the adiabatic shell method.[30] In this approach, a small fraction of the core mass (0.2 a.u. for oxygen in this work) is assigned to the shells, and their motion, controlled by conventional equations of motion, follows the ionic motion adiabatically. Starting from a configuration where all the shells have been relaxed, with no vibrational energy in the core-shell springs, the small mass allows shells to respond quickly to the changing environment so that (almost) no net force acts on them: this is a necessary condition in order to calculate accurate forces on the ion cores. Ideally, due to the low shell mass, no energy exchange between the core-shell spring and the other

TABLE III. Teter potential parameters.

	Buckingham potential			b/r^n	
	A (eV)	ρ (Å)	C (eV Å^6)	b (eV)	n
$O^{1.2-}$-$O^{1.2-}$	2029.22040	0.343645	192.28	44.67287	3.64673
$O^{1.2-}$-$Si^{2.4}$	13702.9050	0.193817	54.681	25.503	4.79
$O^{1.2-}$-$Na^{0.6}$	4383.75550	0.243838	30.700	43.4528	3.598
$O^{1.2-}$-$Ca^{1.2}$	7747.18340	0.252623	93.109	67.0644	3.42435

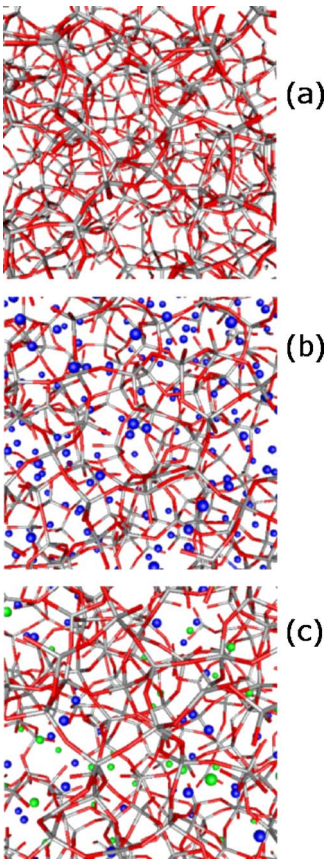

FIG. 1. (Color online) Snapshots of equilibrated glass structures: (a) SiO_2; (b) $30Na_2O$-$70SiO_2$; (c) $10Na_2O$-$15CaO$-$75SiO_2$. Si and O atoms are represented as light and dark sticks, respectively, whereas Na and Ca atoms are represented as dark and light spheres.

degrees of freedom should occur as the frequency of the spring is well above the ionic frequencies. However, a slow leakage usually occurs and the "internal" temperature of the core-shell vibration tends to increase, although at a very low rate.[30] In order to avoid a significant heating of the core-shell degree of freedom over relatively long time scales (above 100 ps), in the present simulations a frictional damping term was added to the core-shell spring force, and the corresponding energy loss was balanced by controlling the system temperature through a Berendsen thermostat; no significant drift in the total energy resulted, with rms fluctuations of less than 0.005%. Cubic periodic boundary conditions are used and the short-range interactions were cut off at 8 Å, whereas the Ewald method[36] was used for summation of the long-range Coulomb interactions with a real-space cutoff of 12 Å; the time step was set to 0.2 fs.

The interaction pair potential between ions i and j consists of a short-range Buckingham term (representing repulsive and dispersive interactions) plus the long-range electrostatic contribution,

$$E_{ij}(r) = A_{ij}e^{-r/\rho_{ij}} - C_{ij}/r^6 + q_i q_j/r, \tag{2}$$

where A_{ij}, ρ_{ij}, and C_{ij} are the Buckingham potential parameters, and q_i is the charge of ion i. Coulombic forces act between all species, whereas the Buckingham potential is applied to the pair interactions involving oxygen: it is customary in most force fields for SiO_2 to exclude short-range forces between Si and other cations, since Si ions are shielded by the oxygen atoms surrounding them. In addition to these two-body terms, in the Sanders potential three-body forces are included to control the O-Si-O angle through a harmonic potential,

$$E_{\mathrm{OSiO}}(\theta) = \frac{1}{2}k_{3b}(\theta - \theta_0)^2, \tag{3}$$

where θ_0 is the tetrahedral angle (109.47°) and k_{3b} is the bending force constant. The Sanders potential (or potentials derived from it) has been successfully used in modeling complex inorganic materials, including zeolites and aluminophosphates.[37–41]

For the modified Na and Ca silicate glasses, several previously published potentials for Na-O and Ca-O interactions, based on the Sanders potential, were tested, but none of them were found to be completely reliable in reproducing the main structural features of sodium- and soda-lime silicate glasses. Therefore we decided to obtain a new set of potential parameters by fitting to the structure of $Na_2Ca(SiO_3)_2$ (Ref. 42) and $Na_2Ca_2(SiO_3)_3$.[43] The first is the only crystal phase found upon crystallization of $25Na_2O$-$25CaO$-$50SiO_2$ glass,[44] and the main crystal phase identified upon crystallization of a typical Bioglass composition,[45] whereas the latter is the crystal phase in bioactive P_2O_5-Na_2O-CaO-SiO_2 glass ceramics.[46] These structures consist of approximately circular six-membered rings of silicate tetrahedra, connected by Na and Ca ions. The GULP code[47] was employed to derive the potential parameters, with the parameters for O-O and Si-O interactions held fixed at the values of the original Sanders potential. The derived potential parameters are listed in Table I, whereas Table II shows the optimized cell parameters obtained with this potential model.

The rigid-ion, partial charge potential of Teter,[48] slightly modified to improve the silicon coordination number,[49] was used both to obtain the initial glass structures for the simulations with the shell-model potential, and to provide structural data for comparison. The Teter potential parameters, listed in Table III, were obtained by fitting to a large number of crystal structures. Recent work[48–51] has employed the Teter potential to model pure silica and sodium silicate glasses, showing that the quality of its reproduction of structural properties is very close to the BKS potential[52] (which is probably the most used partial-charge potential for glass simulations), but with an improved silicon coordination number. Due to the use of partial ionic charges, a three-body angular term is not needed in the Teter potential, and the short-range potential is in the Buckingham form. In order to avoid problems related to the divergence of the power term in the Buckingham potential at short distances, in the high-temperature simulations the Buckingham potential was smoothly switched to an exponential B/r^n repulsive term for short r.[53] For the runs with the Teter potential, a longer time step (2 fs) could be used, and the same cutoffs as for the shell model (SM) runs were employed.

TABLE IV. SiO_2 glass structure. Distances in Å, angles in degrees.

	SM0	SM1	T	CP-LDA[a]	CP-GGA[a]	Expt.
ρ (g cm^{-3})	2.330 (+5.9%)	2.327 (+5.8%)	2.279 (+3.6%)	2.37-2.45 (+7.7–11%)	2.24-2.33 (+1.8–5.9%)	2.20
$r_{Si\text{-}O}$	1.610	1.611	1.615	1.62	1.63	1.610[b]
$r_{O\text{-}O}$	2.63	2.63	2.61	2.65	2.67	2.63[c]
$r_{Si\text{-}Si}$	3.11	3.11	3.16	3.10	3.105	3.08[c]
$\theta_{O\text{-}Si\text{-}O}$	109.2(13)	109.3(12)	108.4(13)	109.5(12)	109.5(13)	109.7(10.6)[2]
$\theta_{Si\text{-}O\text{-}Si}$	145(36)	145(38)	156(35)	149(33), 145(31)[g]	147(33)	144(38),[d] 147(35),[e] 142–151[f]
$CN_{Si\text{-}O}$[h]	4	4	3.99			
$CN_{O\text{-}Si}$	2	2	2			
$CN_{O\text{-}O}$	6.25	6.25	6.07			
$CN_{Si\text{-}Si}$	4.02	4	4			
R_x (%)	5.4%	5.2%	6.1%			

[a]Reference 22.
[b]Reference 63.
[c]Reference 59.
[d]Reference 64.
[e]Reference 65.
[f]Reference 66.
[g]Reference 23.
[h]Coordination number, cutoffs: O-O 3 Å; Si-O 2 Å; Si-Si 3.4 Å.

B. Glass preparation

The three systems studied here are pure silica glass (N =1500 atoms), and two modifications: 30% Na_2O and 10% Na_2O-15% CaO (N=1500 and 1425 atoms, respectively). Snapshots of the three structures are shown in Fig. 1. The glass preparation procedure was as follows: the initial configuration was generated by randomly inserting the appropriate number of ions into a cubic simulation cell whose volume was chosen to reproduce the experimental density of the glass at room temperature. Unphysical overlaps were avoided by defining distances of closest approach between each pair of atomic species, 10–15 % shorter than their optimal distance (that is, the typical distance observed in the crystalline silicates); a new random particle i was inserted in the box only if all its R_{ij} interatomic distances were larger than the predefined cutoffs. Using the Teter potential, the system was then heated to 6000 K and kept at this temperature for 100 ps. Then, the liquid was continuously cooled to 300 K, at a 10 K/ps cooling rate, in 570 ps. A 100 ps equilibration run in the NVT ensemble followed, before the final production run of 200 ps. The final configuration of the Teter run was used to start the shell-model run: the shells were initially relaxed through a short minimization run, then a 100 ps run in the NVT ensemble at T=300 K was carried out, where the last 80 ps were considered for structural analysis.

TABLE V. % Q^n distributions and coordination: SiO_2 glass.

	Q^2	Q^3	Q^4	Q^5	O^1	O^2	O^3	Si^3	Si^4	Si^5
SM0	0	0.5	99.1	0.4	0.01	99.98	0.01	0.4	99.2	0.4
SM1	0	0.8	99.2	0	0.2	99.8	0	0.4	99.6	0
Teter	0.2	2.4	97.4	0	0.5	99.3	0.2	0.6	99.4	0

The use of the Teter potential to generate the initial glass structure deserves some comments. The overall simulation time required to prepare a glass sample is about 1 ns in each case, and we found it more convenient to use the Teter potential in this phase: the need of a shorter time step and the larger number of species in the simulation box for the shell model require a much longer CPU time (by about an order of magnitude) for the same task. Switching to the SM allows for local relaxation of the glass structure at short and medium range, but not for longer-range relaxations involving significant global changes in the network connectivity. For instance, the initial Q^n-species distribution[54] generated with the Teter potential is largely maintained in the SM simulations. There are some advantages in using exactly the same initial structure when comparing the performances of rigid-ion and SM potentials: for instance, any difference in the short-range environment of each ion will be associated with the different potential and not to a (possibly) different glass sample. The effect of using the SM also for generating the glass structure was checked in the case of the sodium silicate glass, for which experimental data are available: the Q^n distribution of the SM-made sodium silicate glass turns out to be significantly closer to the experiment than the corresponding Teter-made glass (see also the discussion in Sec. III D 2). The glass preparation procedure using the SM potential was the same as with the Teter potential: (i) 100 ps high-T trajectory, started from a random initial structure; (ii) cooling at 10 K/ps to 300 K; (iii) 100 ps equilibration followed by a 200 ps production run. In the high-temperature simulations,

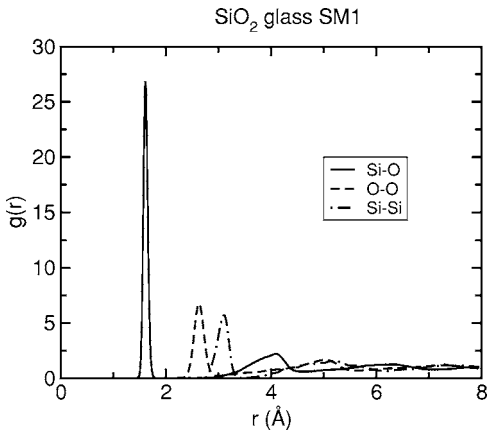

FIG. 2. Radial distribution functions for pure silica glass, SM1 potential.

the Si-O and O-O Buckingham potentials were modified at very short distances in the same way as was done for the Teter glass generation.

C. Car-Parrinello simulations

Accurate structural data on the soda-lime silicate glass were obtained from CPMD, which has already been shown to be reliable in modeling glassy systems.[21–25] The high accuracy obtained from the explicit treatment of the electronic structure is paid for in terms of limited system size and trajectory length. The size of the system and computational procedure were similar to those in previous CPMD studies:[22,24,25] 114 atoms of a $10Na_2O$-15CaO-$75SiO_2$ composition were placed randomly in a periodic cubic box of side 11.655 Å, corresponding to the experimental density of 2.503 g cm^{-3}. Using the Teter potential, the system was heated to 7000 K for 40 ps and then continuously cooled to 300 K in 670 ps, at 10 K/ps nominal cooling rate. Finally, a 200 ps NVT run and 200 ps NVE run were carried out; these long times were used to ensure that the relatively small system achieved full equilibration. The final structure was then used as a starting point of the CPMD simulation, with initial velocities set to zero in order to limit the initial heating of the system due to the switch to the *ab initio* description.[24] CPMD runs were carried out using the CP code included in the Quantum-ESPRESSO package,[55] using the PBE exchange-correlation functional[56] and ultrasoft pseudopotentials[57] for all atomic species, explicitly including semicore shells as valence states for Na and Ca. The accuracy and transferability of the pseudopotentials were extensively tested by comparing the optimized structure of several molecules and crystals containing Na, Ca, Si, and O atoms with the corresponding experimental values, as well as with the corresponding theoretical values calculated with similar approximations. Plane-wave basis set cutoffs for the smooth part of the wave functions and the augmented density were 30 and 200 Ry, respectively, with which convergence was reached for the test calculations discussed above. $\boldsymbol{k}$ sampling was restricted to the Γ point. The time step and fictitious electronic mass were set to 0.1694 fs and 700 a.u., respectively, and a trajectory of 70000 steps (11.8 ps) was carried out, of which the last 50000 steps were used for statistical analysis. After the initial quenching, the temperature of the CPMD run spontaneously increased to ~300 K in 30 fs, and averaged to 295 K over the whole trajectory.

III. RESULTS AND DISCUSSION

A. Silicon coordination

The SM led to a significant fraction (up to 5%) of fivefold-coordinated Si atoms (Si^5) when the modifier cations are included (simulations labeled SM0 in Tables VII and IX). Note that in the initial configuration, generated with the modified Teter potential, no such defects were present, but they are irreversibly formed soon after the potential is switched to the shell model. Although the appearance of these defects had already been observed in simulations using other potentials,[58] experimentally they are only found at relevant concentrations in alkali-metal glasses prepared under high pressure.[59] We considered the possibility that constraining the density to the experimental value in our simulations could result in high pressures imposed on the glasses, in turn leading to the formation of defects. However, a similar percentage of Si^5 defects was formed in test runs carried out at the theoretical density, that is, with the cell volume relaxed to the average volume of a constant-pressure (isotropic NPT) run. This occurrence thus ruled out the above hypothesis, pointing instead to an intrinsic limitation of the SM potential in reproducing the silicon coordination in the presence of modifier cations. The geometry of a Si^5 defect is a trigonal bipyramid, characterized by ~90° O-Si-O angles, which appear as a corresponding tail in the O-Si-O bond-angle distribution (BAD).[58] In order to bias our model against the formation of these defects, we increased the value of the O-Si-O bending force constant, in such a way as to make angles around 90° energetically unfavorable. Moreover, we replaced the raw harmonic form of the three-body potential with a screened harmonic form,

$$E_{\mathrm{OSiO}'}(\theta) = \frac{1}{2}k_{3b}(\theta-\theta_0)^2 \exp[-(r_{\mathrm{Si\text{-}O}}/\rho + r_{\mathrm{Si\text{-}O}'}/\rho)], \quad (4)$$

where $r_{\mathrm{Si\text{-}O}}$ and $r_{\mathrm{Si\text{-}O}'}$ represent the distance between the cen-

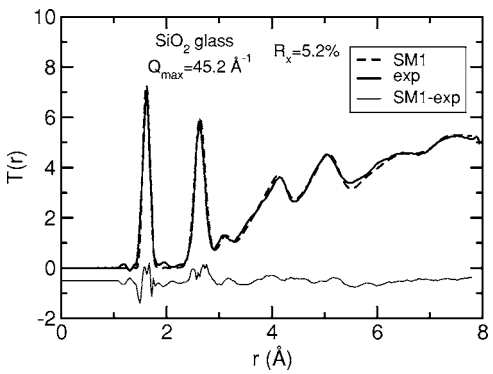

FIG. 3. Total distribution function (broadened using the experimental $Q_{\max}=45.2$ Å^{-1}) obtained from the MD simulation with SM1 potential (dashed line), compared with the neutron diffraction data (full line).

TABLE VI. $30Na_2O$-$70SiO_2$ glass structure. Distances in Å, angles in degrees.

	SM0	SM1	*T*	CP (NS4)[a]	Expt.
ρ (g cm^{-3})	2.572 (+4.2%)	2.516 (+2.0%)	2.514 (+1.9%)		2.466
$r_{Si\text{-}O}$	1.625	1.625	1.614	1.63	1.62[b,c]
$r_{O\text{-}O}$	2.65	2.65	2.61	2.66	2.61[c]
$r_{Si\text{-}Si}$	3.11	3.1	3.15	3.06	3.06[c]
$r_{Na\text{-}O}$	2.33	2.33	2.39	2.28	2.30,[d,e] 2.32,[f] 2.34,[b] 2.45[c]
$r_{Na\text{-}Na}$	3.27	3.24	2.94	3.0	3.2–3.4[c]
$\theta_{O\text{-}Si\text{-}O}$	109.5(15)	109.9(13)	108.7(11)	109(15)	
$\theta_{Si\text{-}O\text{-}Si}$	139(28)	140(31)	150(33)	141(25)	
$\theta_{O\text{-}Na\text{-}O}$	59–92	59–91	55–97		
$CN_{Si\text{-}O}$[g]	4.05	4.00	4		
$CN_{O\text{-}Si}$	1.67	1.65	1.65		
$CN_{O\text{-}O}$	5.35	5.33	5.07		
$CN_{Si\text{-}Si}$	3.26	3.18	3.16		
$CN_{Na\text{-}O}$	5.38	5.33	5.35	5.4±1.1	
$CN_{Na\text{-}Na}$	7.1	7.2	7.5		
R_x (%)	5.1%	4.6%	5.8%		

[a]Reference 24.
[b]Reference 70.
[c]Reference 6.
[d]Reference 4.
[e]Reference 91.
[f]Reference 71.
[g]CN cutoffs: O-O 3 Å; Si-O 2 Å; Si-O 3.4 Å; Na-O 3.1 Å; Na-Na 5 Å.

tral Si atom and the two neighbor oxygens O and O′, respectively. The screening exponential factor damps three-body forces where the O-Si-O angle involves long Si-O distances. This enables a smoother cutoff of the angular term, compared to the raw harmonic potential: using the latter, the maximum distance R_{max} at which the three-body term acts had to be reduced to 1.9 Å in order to avoid instabilities in the dynamics when a pair of atoms crossed the R_{max} cutoff. On the other hand, the use of the damping term allows us to extend the cutoff Si-O distance to 2.5 Å without any problems, as the angular forces are smoothly turned on.[60] Using ρ=1 Å, taking into account the screening exponential, a value of k_{3b}=100 eV rad^{-2} roughly corresponds to doubling the original bending constant for typical Si-O distances of 1.6 Å. With these parameters (simulations denoted as SM1 hereafter), significant improvements in the coordination are obtained for the modified glasses, with a percentage of Si^5 close to 0%. The improvements are seemingly connected both to the higher effective spring constant, which makes the fivefold coordination around silicon less favorable, and to the damping term. In fact, the longer Si-O cutoff allowed by the damping exponential enables us to apply (damped) three-body forces also to O-Si-O triads, which would not otherwise (that is, using the raw harmonic potential) satisfy the conditions to employ the three-body term. The occasional occurrence of these situations during the dynamics with the raw harmonic potential would lead to the formation of stable Si^5 species, which would be difficult to remove subsequently.

TABLE VII. % Q^n distributions and coordination: $30Na_2O$-$70SiO_2$ glass. The initial glass structure for the MD runs is obtained using the Teter potential, apart from SM1*, which was started from an initial glass structure obtained using the SM1 potential.

	Q^1	Q^2	Q^3	Q^4	Q^5	O^0	O^1	O^2	O^3	Si^3	Si^4	Si^5
SM0	0.9	15	47.6	33	3.5	0.1	33.3	66.7	0	0	95.7	4.3
SM1	0.9	15.5	51.5	32.1	0	0.1	35.1	64.8	0	0.01	99.95	0.05
SM1*	0.3	10.6	63.7	25.4	0	0	35.3	64.7	0	0	99.96	0.04
Teter	1.1	16	49.8	33.1	0	0.1	35.1	64.8	0	0	100	0
Expt.[a]	0	8	70	22	0							

[a]Reference 92.

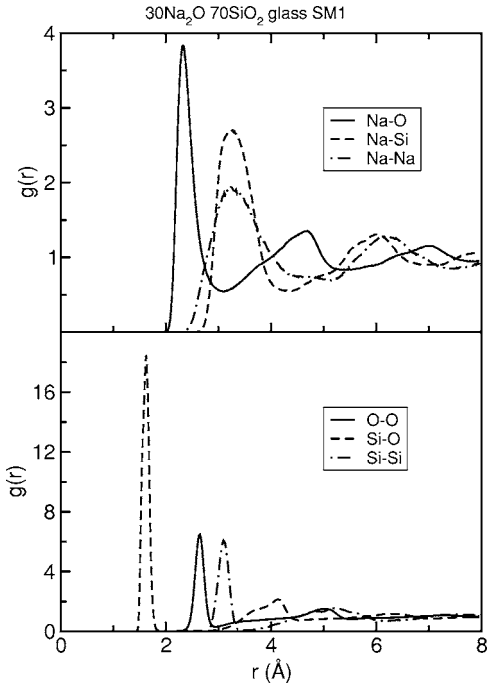

FIG. 4. Radial distribution functions for the $30Na_2O$-$70SiO_2$ glass calculated with the SM1 potential.

B. Theoretical densities

Previous work[58] had shown that the BKS potential yields correct densities, but the rigid-ion potential by Vessal *et al.*,[61] which employs full ionic charges and three-body angular terms, did not reproduce the experimental density accurately.[58,62] This seemed to point out an intrinsic limitation of full-charge potentials in reproducing the correct density of these systems. In Tables IV, VI, and X, the theoretical densities, calculated using the average cell volume of a 40 ps NPT simulation, are compared with the experimental densities of the simulated systems, for both Teter and the new SM potentials. In general, the differences are small: the Teter potential performs slightly better for the pure silica glass, and for the modified glasses both the SM (especially SM1) and the Teter potentials yield densities in very good agreement with the experimental ones. In other words, the inclusion of shells and the explicit approximate treatment of polarization effects reduces the internal strain of the bulk glasses compared to an equivalent rigid-ion potential with full ionic charges and three-body forces, making the SM more suitable for surface simulations, which require the bulk structures to have reasonable densities under zero pressure.

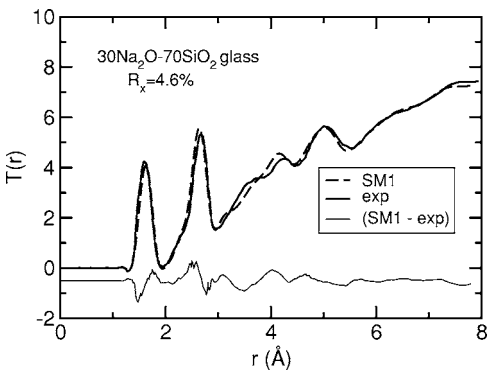

FIG. 5. Total distribution function (broadened using the experimental Q_{max}=22.88 Å^{-1}) obtained from the MD simulation with SM1 potential (dashed line), compared with the neutron diffraction data (full line).

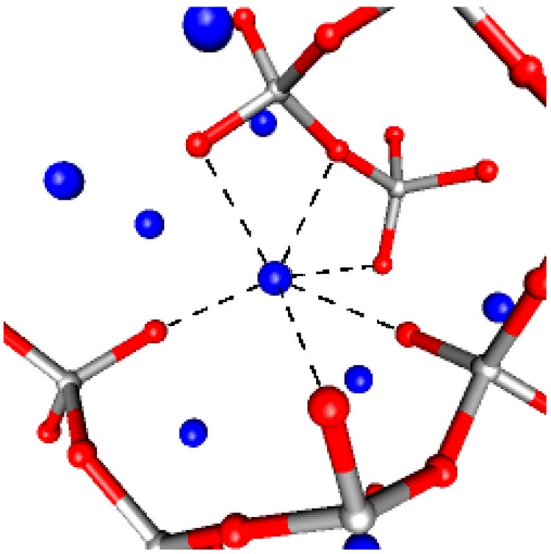

FIG. 6. (Color online) Enlargement of a snapshot taken from the $30Na_2O$-$70SiO_2$ run, showing the local structure around sodium. Dashed lines connect the central Na ion to the six closest oxygen atoms. Na are pictured as dark spheres, Si and O are represented as ball-and-sticks.

C. Pure silica glass

Table IV lists the structural parameters calculated for the pure silica glass from the simulations with SM0 (original bending term in the Sanders potential), SM1 (modified bending term), and Teter potential, compared to the available experimental and *ab initio* data. The larger bending constant does not affect the structure compared to the SM0 potential, besides very small changes in the full width at half-maximum (FWHM) of the O-Si-O and Si-O-Si BAD. The location of the BAD maxima is unaffected, and the same applies to the peaks in the radial distribution functions (RDFs). A similar comparison applies to the modified silicate glasses as well: the modified bending potential does not introduce any structural perturbation, besides improving the coordination statistics.

TABLE VIII. Distances from BO/NBO atoms (Å): $30Na_2O$-$70SiO_2$ glass.

	Si-NBO	Si-BO	Na-NBO	Na-BO
SM1	1.54	1.63	2.31	2.47
Teter	1.57	1.62	2.36	2.62
CP-GGA (NS4 glass)[a]	1.58	1.65		

[a]Reference 24.

TABLE IX. $\%Q^n$ distributions and coordination: $10Na_2O$-15CaO-$75SiO_2$ glass.

	Q^1	Q^2	Q^3	Q^4	Q^5	O^1	O^2	O^3	Si^3	Si^4	Si^5
SM0	0.9	8.5	41.5	45.3	3.8	26.5	73.4	0.1	0	95	5
SM1	0.8	9.9	44.4	44.8	0.1	28.5	71.5	0	0	99.9	0.1
Teter	0.8	10.4	43.5	45.3	0	28.6	71.4	0	0	100	0
CP-GGA	0	20	26.7	53.3	0	28.6	71.4	0	0	100	0

The short-range structure of pure silica glass predicted by SM1, represented in the RDFs of Fig. 2, is in very good agreement with experimental[3,63–66] and Car-Parrinello *ab initio* molecular dynamics (CPMD)[21–23] data. The introduction of shells improves the description of the structure: the R_x factor (as defined in Refs. 58 and 67) of 5.2%, calculated by comparing the simulated $T(r)$ (Ref. 68) in Fig. 3 to the neutron diffraction data of Grimley,[3] is about 1% smaller than the one we obtain with the Teter potential (Table IV); the R_x factor is also significantly improved with respect to the 9.3% value obtained using the corresponding Vessal rigid-ion model,[58] and with respect to the 7.2% yielded by the BKS potential.[58]

The differences with respect to the Teter potential are minimal: a shorter Si-Si distance (3.1 Å) and a corresponding lower average Si-O-Si angle (145°), which are closer both to the experiments and CPMD simulations (see Ref. 69 for a recent discussion of the Si-O-Si BAD in silicate glasses). Although the very low fraction (0.4%) of Si^5 defects present in the SM0 run with the original k_{3b} is completely removed with a higher bending constant (see Table V), it should be remarked that the main benefits of adjusting the three-body potential apply to the modified silicate glasses, and no adjustments to k_{3b} would in principle be needed to model the pure silica glass with the SM0. This point is highlighted in Table IV, showing ideal coordination numbers for Si and O in all runs.

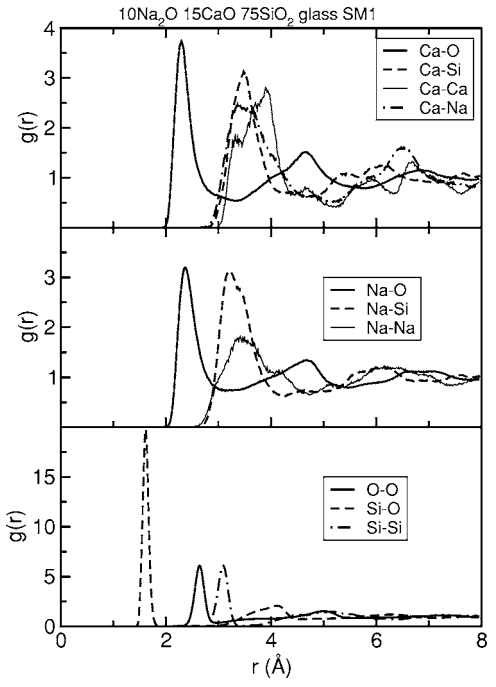

FIG. 7. Radial distribution functions for the $10Na_2O$-15CaO-$70SiO_2$ glass calculated with the SM1 potential.

D. $30Na_2O$-$70SiO_2$ glass

1. Radial and angular distribution functions

Tables VI and VII show that 4.3% of Si^5 are formed with the SM0 potential, but practically all Si atoms are found in perfect (tetrahedral) coordination when we switch to the SM1 potential.

The structure is examined in Table VI, and the RDFs are shown in Fig. 4: in the sodium silicate case, the R_x factor was calculated comparing the broadened $T(r)$ to the neutron diffraction data of Wright,[70] using a maximum Q of 22.88 $Å^{-1}$; the SM yields again a very good match with the experimental structure; the R_x factor of 4.6% with SM1 potential, see Fig. 5, is significantly improved with respect to Teter potential (R_x=5.8%), as well as with respect to BKS and Vessal potentials (5.6% and 6.8%, respectively[58]). As for the pure silica glass, the location of the peaks in the Si-Si RDFs and Si-O-Si BADs shows some minor improvements with respect to the Teter potential, when we compare to previous CPMD[24] simulations and experimental neutron and EXAFS data.[70,71,91] Compared to pure silica glass, the Si-O distance increases with the addition of sodium, as is observed experimentally.[72,73] The increase in Si-O upon addition of sodium is correlated with the shift of Si-O-Si BADs to smaller angles, observed for both the SM and Teter poten-

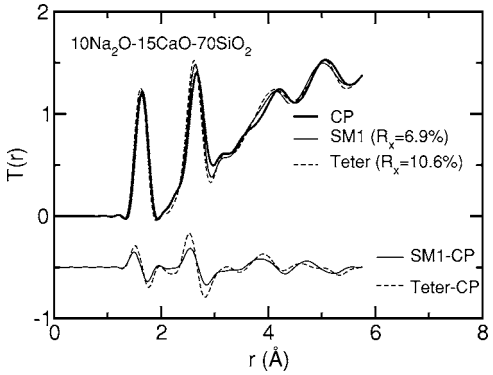

FIG. 8. Top: total distribution function (broadened using Q_{max}=22.88 $Å^{-1}$) obtained from CPMD (full thick line), SM1 potential (full thin line), and Teter potential (dashed line). The functions have been calculated up to half the CPMD cell size (5.8 Å). Bottom: difference between CPMD and SM1 potential (full thin line), and between CPMD and Teter potential (dashed line).

TABLE X. $10Na_2O$-15CaO-$75SiO_2$ glass structure. Distances in Å, angles in degrees.

	SM0	SM1	*T*	CP	Expt.
ρ (g cm^{-3})	2.634 (+5.2%)	2.578 (+3%)	2.564 (+2.4%)		2.503
$r_{Si\text{-}O}$	1.615	1.618	1.610	1.63	
$r_{O\text{-}O}$	2.64	2.64	2.61	2.65	
$r_{Si\text{-}Si}$	3.10	3.09	3.16	3.08	
$r_{Na\text{-}O}$	2.38	2.37	2.39	2.35	
$r_{Na\text{-}Na}$	3.5	3.4	3.25	3.3	
$r_{Ca\text{-}O}$	2.30	2.30	2.37	2.30	
$r_{Ca\text{-}Na}$	3.5	3.4	3.32	3.45	
$\theta_{O\text{-}Si\text{-}O}$	109.6(15)	109.9(13)	108.4(12)	108.7(14)	
$\theta_{Si\text{-}O\text{-}Si}$	141(28)	141(30)	148(36)	137(24)	
$\theta_{O\text{-}Na\text{-}O}$	58–95	58–95	57–89	56–83	
$\theta_{O\text{-}Ca\text{-}O}$	56–85	56–85	56–85	61–80	
$CN_{Si\text{-}O}$[a]	4.06	4	4	4	
$CN_{O\text{-}Si}$	1.74	1.71	1.71	1.71	
$CN_{O\text{-}O}$	5.67	5.62	5.35	5.66	
$CN_{Si\text{-}Si}$	3.47	3.35	3.34	3.44	
$CN_{Na\text{-}O}$	5.8	5.72	5.55	5.6	
$CN_{Ca\text{-}O}$	5.85	5.95	6.2	5.9	
$CN_{Na\text{-}Na}$	2.28	2.31	2.38	3.0	
$CN_{Ca\text{-}Ca}$	1.88	1.98	1.89	2.4	
$CN_{Na\text{-}Ca}$	1.98	1.97	2.06	2.0	

[a]CN cutoffs: O-O 3 Å; Si-O 2 Å; Si-Si 3.4 Å; Na-O 3.1 Å; Na(Ca)-Na(Ca) 5 Å; Ca-O 3.2 Å.

tials; the Si-O-Si BAD peak position for the SM1 potential (140°) is very close to the 141° obtained by CPMD. Note also that the SM predicts a narrower Si-O-Si BAD (the FWHM decreases by 7° with respect to pure SiO_2 glass) upon addition of sodium, which agrees nicely with experimental indications.[74,75]

It is interesting to consider the local order around the sodium atom predicted by the SM, as the relevant Na-O potential was refined for the present work. The first-neighbor Na-O distance of 2.33 Å compares well with the value of 2.28 Å predicted by CPMD simulations,[24] and even better with values between 2.30 and 2.34 obtained in EXAFS and neutron studies.[4,70,71,91] The RMC fit of Zotov *et al.*,[6] on the other hand, gives a longer Na-O distance of 2.45 Å, which is also reflected in a Na-Si distance 0.2 Å longer than the one predicted by our model. The O-Na-O BADs obtained by the SM and Teter potentials are similar, featuring a sharp peak around 60° and a broader peak around 90°.

It is well established that the introduction of modifier cations *M* disrupts the tetrahedral network, by breaking Si-O-Si linkages and hence forming Si-O bonds where the oxygen is not bridging between two tetrahedra. Each modifier cation is usually linked to several BO and NBO, see Fig. 6: the peak around 90° in the O-Na-O BAD results from NBO-Na-NBO groups. Table VII shows that the number of NBOs (O^1 in the table) created with the introduction of Na cations in the silicate network matches almost exactly the number of Na atoms in the simulation cell; each NBO is bonded to a Si and weakly coordinated to ~3 Na atoms. The coordination number of sodium (calculated using the first minimum at 3.1 Å in the Na-O RDF as cutoff radius) is 5.33 (of which 60% NBO) for the SM and 5.35 (of which 64% NBO) for the Teter potentials, which compare favorably with the CPMD value of 5.4±1.1. The RDFs calculated separately for BO and NBO (peak positions reported in Table VIII) show that Si-BO bonds are 0.09 Å (0.05 Å) longer than Si-NBO in the SM (Teter) potential, in good agreement with the difference observed in CPMD simulations (0.07 Å).[24]

2. Q^n-species distribution

The environment around Si atoms can be described by the Q^n notation,[54] where *n* is the number of BOs in the first coordination shell of Si. Only Q^4 species are present in pure silica glasses, while Q^2 and Q^3 species are formed in the modified glasses. According to the binary model,[76] Q^{n+1} species will completely transform into Q^n before Q^{n-1} can be formed; however, NMR experiments tend to show inadequacies of this model and point to the existence of several different Q^n species.[77,92] As mentioned above, no significant changes to the Q^n-species distributions in the glass generated through the Teter potential are expected after switching to the SM. The sodium silicate sample shows a prevalence of Q^3 species followed by Q^4 and Q^2 (Table VII). The presence of more than two Q^n species and their relative ordering agrees with the NMR results for this composition,[92] but the experimental data show a larger percentage (around 70%) of Q^3. This difference could be somewhat related to the necessarily

TABLE XI. Distances from BO/NBO atoms: $10Na_2O$-$15CaO$-$75SiO_2$ glass (Å).

	Si-NBO	Si-BO	Na-NBO	Na-BO	Ca-NBO	Ca-BO
SM1	1.54	1.625	2.31	2.48	2.30	2.64
Teter	1.57	1.615	2.36	2.64	2.37	2.62
CP-GGA	1.59	1.64	2.31	2.62	2.30	2.54

much higher cooling rate used in our glass-generation procedure compared to the experiment;[50] however, we carried out a lengthy glass-generation procedure using only the SM1 model, and the resulting Q^n distribution, denoted SM1* in Table VII, is now much closer to the experimental one. It thus appears that the shell model improves the description of the experimental glass structure (although at a higher computational expense), especially for what concerns the connectivity of the tetrahedral network. Apart from the Q^n percentages, we checked that the distances and angles reported in Table VI for the SM1 glass match very closely those of the SM1* sample, as is expected since the short-range order should not depend directly on the preparation history. The only observable variations are in structural properties more directly affected by the Q^n relative abundances: the Si-Si distance (0.05 Å shorter in the SM1* glass) and the Si-O-Si angle (5° smaller in the SM1* glass).

E. $10Na_2O$-$15CaO$-$75SiO_2$ glass

To our knowledge, only a previous MD study, using the BKS potential, involved the $10Na_2O$-$15CaO$-$75SiO_2$ glass,[79] whereas no neutron diffraction data or *ab initio* calculations

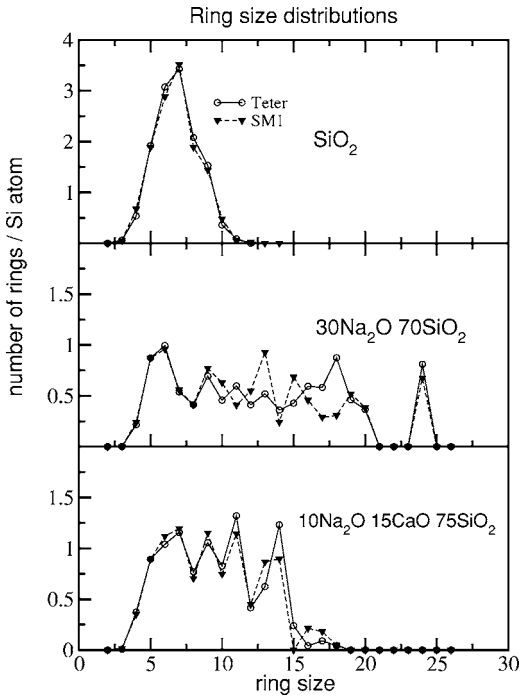

FIG. 9. Ring size distributions calculated from the runs with the SM1 (full triangles) and Teter (circles) potentials.

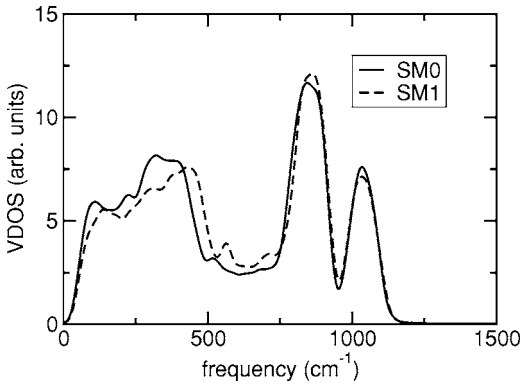

FIG. 10. VDOS of pure silica glass, SM models.

of this structure are as yet available; in this work, accurate reference data on the local structure were therefore obtained from CPMD simulations of a smaller sample. As for the sodium silicate glass, Table IX shows that adjusting the bending potential (run SM1) completely removes oddly coordinated silicon atoms, whereas a relevant fraction (5%) of these defects were formed in the SM0 run; note also that no Si^5 or O^3 atoms are formed in our CPMD run, which confirms that the occurrence of these defects is unlikely at standard temperatures and pressure. The different Q^n distribution of the sample used in the CPMD simulation is probably related to the smaller system size.[78] The RDFs for the SM1 run are shown in Fig. 7, and the structural data are collected in Table X. Although no experimental total correlation function was available in this case, we calculated the *ab initio* $T(r)$ from the CPMD trajectory, using the same approach as for the pure silica and sodium silicate glasses, and used it as reference. The comparison with the $T(r)$ calculated for the SM1 and Teter models and the corresponding R_x factors (reported in Fig. 8) confirms the overall better performances of the shell model in this case as well.

The main structural features predicted by the SM and Teter potentials are rather similar to those of the sodium silicate glass; the absence of major modifications due to the replacement of sodium with calcium is in agreement with the previous MD simulation using the BKS potential.[79] As for the pure silica and sodium silicate glasses, small improvements in the SM with respect to the Teter potential concern the Si-Si distance and Si-O-Si angle: in general, the glass

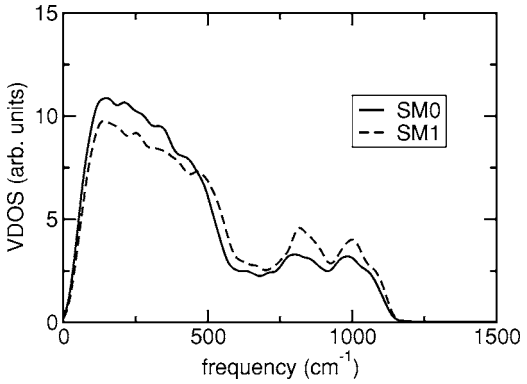

FIG. 11. VDOS of sodium silicate glass, SM models.

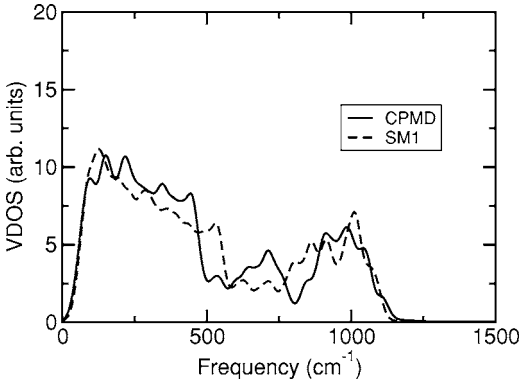

FIG. 12. VDOS of soda-lime silicate glass, CPMD and SM models.

structures predicted by SM and CPMD are in very good agreement. The Ca-O distance is slightly shorter than the Na-O distance in both empirical models, and both distances are closer to the CPMD data in the case of the SM potential. Both Na-O and Ca-O distances fall in the lower range of the distances observed in crystalline $Na_2CaSi_2O_6$.[42] With the SM1 potential, each Na ion is coordinated to 5.7 oxygens, of which 49% are NBO, whereas the Ca ions show a net preference for NBO coordination:[79] 69% of the 5.9 oxygens in Ca first coordination shell are NBO. With the Teter potential, each Na ion is coordinated to 5.5 oxygens, of which 54% are NBO, and the Ca ions show a similar preference for NBO coordination: 71% of the 6.2 oxygens in the calcium first coordination shell are NBO. This greater preference of Ca for NBO coordination is quantitatively similar to what is observed with the BKS potential;[79] previous MD simulations of a different soda-lime silicate glass composition[44] also showed a higher fraction of NBO in the Ca coordination shell, although their relative BO-NBO percentages differ significatively from ours, due to the different glass composition. A Ca-O total coordination number higher than Na-O is also apparent in all our simulations, however the difference is less marked in the SM and CPMD simulations. Compared to the CPMD results, the SM model yields exactly the same Na-NBO (2.31 Å) and Ca-NBO (2.30 Å) distances, and fairly accurate Na-BO and Ca-BO distances (Table XI). The Teter potential predicts a Na-BO distance closer to the *ab initio* value. Si-BO (-NBO) distances of 1.625 Å (1.54 Å) are also close to the CPMD values.

A recent NMR study[80] examined the distribution of Ca and Na ions around bridging and nonbridging oxygens in soda-lime silicate glasses with the same mol% of SiO_2 (75%) as our system, but slightly different fractions of Na_2O and CaO. The NMR data evidenced interactions between network-modifying cations and the bridging oxygen network, as well as extensive mixing of Ca and Na around NBO. We directly calculated the distribution $N(i,j)$ of NBO atoms coordinated to i Na and j Ca ions from the SM1 trajectory, and the average percentages are $N(1,1)=28\%$, $N(2,0)=5\%$, $N(0,2)=16\%$ for NBO coordinated to two ions; $N(1,2)=14\%$, $N(2,1)=16\%$, $N(3,0)=5\%$, $N(0,3)=3\%$ for threefold coordination. The higher percentage of "mixed" (that is, including both Na and Ca) coordination shells, with respect to coordination shells involving only one type of ion, points out some preference for Na-Ca pairing around NBOs.

F. Distribution of ring sizes

The distribution of primitive ring sizes, shown in Fig. 9 for the SM1 and Teter runs, has been calculated with the algorithm proposed in Ref. 81; the two models yield similar ring size distributions, with some differences only for the sodium silicate glass. For the pure silica glass, the ring size distribution extends from 3- to 11-membered rings, with a maximum around 6–7. The disruption of the network of tetrahedra due to introduction of sodium results in a decrease of the number of 6-membered rings from above three to about one per Si atom, and in the appearance of larger rings, up to 20-membered; it is likely that the occurrence of the isolated peak at the 24-membered ring is related to the limited cell size.[81] The ring size distribution for the soda-lime glass is narrower, with a maximum ring size around 15, but otherwise similar to the sodium silicate, with a first maximum of about one 6-membered ring per Si atom.

G. Vibrational properties

In a previous work,[82] the vibrational density of states (VDOS) of amorphous SiO_2 was calculated using several potentials including the Sanders shell model; the latter yielded a rather different and inaccurate vibrational spectrum compared to other potentials. In particular, two common partial charge potentials such as Tsuneyuki[83] and (especially) BKS[52] yielded fairly accurate VDOS spectra, despite a less satisfactory agreement with the experimental VDOS at intermediate frequencies.[82,84,85] The poor performance of the SM in Ref. 82 is rather unexpected, as the elastic and dielectric constants of quartz were fitted parameters in the model;[34] however, the potential described in Table 1 of Ref. 82 does not match exactly the Sanders model (a Si-O stretching term is included). Indeed, the VDOS (shown in Fig. 10) for the pure silica glass modeled with the SM potential, calculated as the Fourier transform of the mass-weighted velocity autocorrelation function,[86] is different and much improved with respect to the one reported in Ref. 82.

The SM0 yields a reasonably accurate VDOS [compared with the experimental inelastic neutron scattering (INS) values[2] of ~400, 800, and 1100 cm^{-1}], with three main bands centered at 370, 830, and 1030 cm^{-1}; modifying the bending term (potential SM1) has no effect on the location of the two higher-frequency peaks, whereas the lowest frequency peak is shifted to 440 cm^{-1}. The frequencies obtained for the SM1 potential are thus in good agreement with the IR spectrum calculated with the PIM method,[27] which shows three bands at 463, 802, and 1080 cm^{-1} (note that VDOS and IR intensities are not directly comparable). An additional small peak at 560 cm^{-1} (520 cm^{-1} with the SM0 potential) is present in our calculated VDOS, which has also been observed around 600 cm^{-1} in VDOS calculated through CPMD simulations.[21,84] Overall, although the splitting of the high-frequency peak is not reproduced, the VDOS at intermediate

frequency is better represented in the SM model than the BKS potential.

For the sodium silicate glass, Fig. 11 shows a similar effect. In this case no INS spectra exist, to the best of our knowledge; the main peaks in the Raman spectrum of a NS3 glass[87] are found around 500, 800, and 1100 cm^{-1}. Model calculations by Zotov *et al.*[88] for NS4 glass show that the VDOS increases in intensity in the 200–400 cm^{-1} region, correlated to the presence of NBO. This same increase is present to a larger extent in our calculated VDOS, as a larger number of NBOs is present in our glass composition compared to the NS4 glass; this intensity tends to mask the first peak above 400 cm^{-1}. The locations of the two other main bands are similar to the ones found for the pure silica glass, as are also observed for the NS4 glass.[88] The location of the high-frequency peak at 1000 cm^{-1} with a shoulder at 1090 cm^{-1} agrees fairly well with recent CPMD calculations for sodium tetrasilicate,[89] despite the different intensities, which are related to the different composition. The midfrequency band at 820 cm^{-1} is shifted to high frequencies compared to the CPMD data, but a similar blueshift was previously observed with a classical valence force field potential fitted using experimental vibrational frequencies of crystalline silica and sodium silicates.[89]

Figure 12 shows the VDOS of the soda-lime silicate glass obtained using CPMD and the SM1 potential. The VDOS for the SM1 potential was calculated from an MD trajectory of the same small system used for the CP run, in order to minimize differences in the spectrum related to the small size of the glass sample used in the *ab initio* simulation. The low- and high-frequency bands are broader, compared to the sodium silicate glass; as for the sodium silicate glass, the SM1 model yields a blueshift of the band at intermediate frequencies, which tends to partially overlap the high-frequency region. On the other hand, the low- and high-frequency bands are in better agreement.

To sum up, the vibrational properties of glasses modeled through the SM are fairly adequately represented, and no significant distortions are induced by the modified three-body term. An intrinsic difficulty to reproduce correctly the intermediate region of the vibrational spectrum of glasses, which seems to be common to most force fields, is observed for the modified glasses.

IV. CONCLUSIONS

We have developed an empirical potential (SM1) for the simulation of modified silicate glasses, using full ionic charges, with a SM approach to represent polarization effects. To our knowledge, no previous applications of the SM to MD simulations of glasses have been reported. The performances of the potential have been thoroughly checked and compared with other rigid-ion potentials, and with available experimental and *ab initio* theoretical data. The main points can be summarized as follows: (a) the use of the SM removes some problems associated with the use of formal ionic charges and three-body angle-bending terms: in particular, the experimental density of the modified glasses is reproduced very well, with both the rigid-ion and SM potentials; (b) the rigid-ion Teter potential performs rather well in describing the complex structural properties of modified silicate glasses; however, we have shown that the Si-O-Si angle (and the related Si-Si distance) predicted by the SM1 potential is closer to the predictions of experiments and *ab initio* MD, and significant improvements in the description of the local environment surrounding Na and Ca ions are also obtained with the shell model; (c) vibrational properties are fairly satisfactorily reproduced, despite some apparent discrepancies in the intermediate frequency region for the modified glasses, which seem to be common to other force fields as well; (d) the sodium silicate glass generated using the shell model shows a Q^n distribution significantly closer to the experiment than the same glass generated with the rigid-ion potential. The last point appears particularly important, given the strong influence of the network connectivity on the glass physical properties, such as the solubility.[90]

The potential thus combines a reliable representation of the experimental density with an accurate reproduction of the structural and dynamical properties of the modified glasses, which can hardly be obtained with rigid-ion models. The explicit inclusion of polarization effects through the shell model seems to be essential to obtain high structural accuracy, as also confirmed by the *ab initio* MD results, despite the small size of the system used in the CPMD simulations. The higher computational requirements of the SM versus rigid-ion dynamics appear reasonable, in view of the greater versatility warranted by the first. For instance, the potential can be used in the simulation of glass surfaces, where the highly heterogeneous local environment involving varying coordination and distorted local geometries (resulting in ionic charge distributions different from those of the bulk) should be well represented by the shell model. In fact, preliminary calculations appear to confirm the reliability of the potential to model glass surfaces and will be presented in a subsequent paper.

ACKNOWLEDGMENTS

The Engineering and Physical Sciences Research Council, UK, is gratefully acknowledged for financial support (Grant No. GR/S77714/01).

*Electronic address: a.tilocca@ucl.ac.uk

[1] L. L. Hench and O. Andersson, in *An Introduction to Bioceramics*, edited by L. L. Hench and J. Wilson (World Scientific, Singapore, 1993).

[2] J. M. Carpenter and D. L. Price, Phys. Rev. Lett. **54**, 441 (1985).

[3] D. I. Grimley, A. C. Wright, and R. N. Sinclair, J. Non-Cryst. Solids **119**, 49 (1990).

[4] C. Mazzara, J. Jupille, A. M. Flank, and P. Lagarde, J. Phys.

Chem. B **104**, 3438 (2000).
[5] G. H. Wolf, D. J. Durben, and P. F. McMillan, J. Chem. Phys. **93**, 2280 (1990).
[6] N. Zotov and H. Keppler, Phys. Chem. Miner. **25**, 259 (1998).
[7] B. Vessal, G. N. Greaves, P. T. Marten, A. V. Chadwick, R. Mole, and S. Houde-Walter, Nature (London) **356**, 504 (1992).
[8] K. Vollmayr, W. Kob, and K. Binder, Phys. Rev. B **54**, 15808 (1996).
[9] C. Huang and A. N. Cormack, J. Chem. Phys. **93**, 8180 (1990).
[10] A. Takada, P. Richet, C. R. A. Catlow, and G. D. Price, J. Non-Cryst. Solids **345**, 224 (2004).
[11] W. Smith, G. N. Greaves, and M. J. Gillan, J. Chem. Phys. **103**, 3091 (1995).
[12] P. Jund, W. Kob, and R. Jullien, Phys. Rev. B **64**, 134303 (2001).
[13] E. Sunyer, P. Jund, W. Kob, and R. Jullien, J. Non-Cryst. Solids **307**, 939 (2002).
[14] A. Meyer, J. Horbach, W. Kob, F. Kargl, and H. Schober, Phys. Rev. Lett. **93**, 027801 (2004).
[15] P. A. Madden and M. Wilson, Chem. Soc. Rev. **25**, 339 (1996).
[16] T. D. Archer, S. E. A. Birse, M. T. Dove, S. A. T. Redfern, J. D. Gale, and R. T. Cygan, Phys. Chem. Miner. **30**, 416 (2003).
[17] J. S. Lin and C. R. A. Catlow, J. Mater. Chem. **3**, 1217 (1993).
[18] E. Heifets, E. A. Kotomin, and J. Maier, Surf. Sci. **462**, 19 (2000).
[19] P. Zapol, R. Pandey, and J. D Gale, J. Phys.: Condens. Matter **9**, 9517 (1997).
[20] R. Car and M. Parrinello, Phys. Rev. Lett. **55**, 2471 (1985).
[21] J. Sarnthein, A. Pasquarello, and R. Car, Science **275**, 1925 (1997).
[22] R. M. Van Ginhoven, H. Jonsson, and L. R. Corrales, Phys. Rev. B **71**, 024208 (2005).
[23] M. Benoit, S. Ispas, P. Jund, and R. Jullien, Eur. Phys. J. B **13**, 631 (2000).
[24] S. Ispas, M. Benoit, P. Jund, and R. Jullien, Phys. Rev. B **64**, 214206 (2001); S. Ispas, M. Benoit, P. Jund, and R. Jullien, J. Non-Cryst. Solids **307**, 946 (2002).
[25] D. Donadio, M. Bernasconi, and F. Tassone, Phys. Rev. B **70**, 214205 (2004).
[26] M. Wilson and P. A. Madden, J. Phys.: Condens. Matter **5**, 2687 (1993).
[27] M. Wilson, P. A. Madden, M. Hemmati, and C. A. Angell, Phys. Rev. Lett. **77**, 4023 (1996).
[28] M. Wilson and T. R. Walsh, J. Chem. Phys. **113**, 9180 (2000).
[29] B. G. Dick and A. W. Overhauser, Phys. Rev. **112**, 90 (1958).
[30] P. J. Mitchell and D. Fincham, J. Phys.: Condens. Matter **5**, 1031 (1993).
[31] K. P. Schroder, J. Sauer, M. Leslie, C. R. A. Catlow, and J. M. Thomas, Chem. Phys. Lett. **188**, 320 (1992).
[32] F. Bottin, F. Finocchi, and C. Noguera, Surf. Sci. **574**, 75 (2005).
[33] N. H. de Leeuw and S. C. Parker, Phys. Rev. B **58**, 13901 (1998).
[34] M. J. Sanders, M. Leslie, and C. R. A. Catlow, J. Chem. Soc., Chem. Commun. **1984** 1273 (1984).
[35] W. Smith, M. Leslie, and T. R. Forester, Daresbury Laboratory, UK, http://www.cse.clrc.ac.uk/msi/software/DL_POLY *v. 2.15*.
[36] P. P. Ewald, Ann. Phys. **64**, 253 (1921).
[37] K.-P. Schroeder, J. Sauer, M. Leslie, C. R. A. Catlow, and J. M. Thomas, Chem. Phys. Lett. **3**, 320 (1992).
[38] N. H. de Leeuw, F. M. Higgins, and S. C. Parker, J. Phys. Chem. B **103**, 1270 (1999).
[39] G. Sastre, D. W. Lewis, and C. R. A. Catlow, J. Phys. Chem. **100**, 6722 (1996).
[40] Y. M. Channon, C. R. A. Catlow, R. A. Jackson, and S. L. Owens, Microporous Mesoporous Mater. **24**, 153 (1998).
[41] J. D. Gale and N. H. Henson, J. Chem. Soc., Faraday Trans. **90**, 3175 (1994).
[42] H. Ohsato, I. Maki, and Y. Takeuchi, Acta Crystallogr., Sect. C: Cryst. Struct. Commun. **C41**, 1575 (1985).
[43] R. X. Fischer and E. Tillmanns, Acta Crystallogr., Sect. C: Cryst. Struct. Commun. **C43**, 1852 (1987).
[44] G. Lusvardi, G. Malavasi, L. Menabue, and M. C. Menziani, J. Phys. Chem. B **106**, 9753 (2002).
[45] L. Linati, G. Lusvardi, G. Malavasi, L. Menabue, M. C. Menziani, P. Mustarelli, and U. Segre, J. Phys. Chem. B **109**, 4989 (2005).
[46] O. Peitl, E. D. Zanotto, and L. L. Hench, J. Non-Cryst. Solids **292**, 115 (2001).
[47] J. D. Gale, General Utility Lattice Program (GULP), The Royal Institution of Great Britain/Imperial College, 1992–4.
[48] A. N. Cormack, J. Du, and T. R. Zeitler, Phys. Chem. Chem. Phys. **4**, 3193 (2002).
[49] A. N. Cormack, J. Du, and T. R. Zeitler, J. Non-Cryst. Solids **323**, 147 (2003); see also J. Non-Cryst. Solids **351**, 956 (2005).
[50] J. Du and A. N. Cormack, J. Non-Cryst. Solids **349**, 66 (2004).
[51] J. Du and A. N. Cormack, J. Am. Ceram. Soc. **88**, 2532 (2005).
[52] B. W. H. van Beest, G. J. Kramer, and R. A. Van Santen, Phys. Rev. Lett. **64**, 1955 (1990).
[53] V. A. Bakaev and W. A. Steele, J. Chem. Phys. **111**, 9803 (1999).
[54] The Q^n notation denotes SiO_4 tetrahedra with n bridging oxygens; the theoretical Q^n distribution is obtained in our MD trajectories by first determining the local coordination of Si and O atoms at each time step and then identifying and averaging the number of Q^n species.
[55] S. Baroni, A. Dal Corso, S. de Gironcoli, P. Giannozzi, C. Cavazzoni, G. Ballabio, S. Scandolo, G. Chiarotti, P. Focher, A. Pasquarello, K. Laasonen, A. Trave, R. Car, N. Marzari, and A. Kokalj, http://www.pwscf.org/.
[56] J. P. Perdew, K. Burke, and M. Ernzerhof, Phys. Rev. Lett. **77**, 3865 (1996).
[57] D. Vanderbilt, Phys. Rev. B **41**, R7892 (1990).
[58] X. Yuan and A. N. Cormack, J. Non-Cryst. Solids **283**, 69 (2001).
[59] J. F. Stebbins and P. McMillian, J. Non-Cryst. Solids **160**, 116 (1993).
[60] While the tail of the first maximum in the Si-O radial distribution function extends up to 2 Å, occasionally Si-O pairs are found at distances between 2.0 and 2.5 Å, which is between the first and the second coordination shell; the use of R_{max}=2.5 Å together with the damping exponential allows us to apply small, damped angular forces to O-Si-O triads involving these pairs. These forces will gradually and smoothly increase if the O atom eventually moves into the first Si coordination shell.
[61] B. Vessal, M. Amini, D. Fincham, and C. R. A. Catlow, Philos. Mag. B **60**, 753 (1989).
[62] X. Yuan and A. N. Cormack, Ceram. Trans. **82**, 281 (1997).
[63] P. A. V. Johnson, A. C. Wright, and R. N. Sinclair, J. Non-Cryst. Solids **58**, 109 (1983).
[64] R. Mozzi and B. Warren, J. Appl. Crystallogr. **2**, 164 (1969).
[65] H. F. Poulsen, J. Neuefeind, H. B. Neumann, J. R. Schneider, and M. D. Zeidler, J. Non-Cryst. Solids **188**, 63 (1995).
[66] R. F. Pettifer, R. Dupree, I. Farnan, and U. Sternberg, J. Non-

Cryst. Solids **106**, 408 (1988).
[67] A. C. Wright, J. Non-Cryst. Solids **159**, 264 (1993).
[68] In order to obtain a theoretical total correlation function which can be directly compared to the experimental $T(r)$, one has to take into account the broadening in the latter, related to the finite maximum momentum transfer Q_{max} and the consequent use of damping functions in reciprocal space to reduce termination ripples [see R. Lovell, G. R. Mitchell, and A. H. Windle, Acta Crystallogr., Sect. A: Cryst. Phys., Diffr., Theor. Gen. Crystallogr. **A35**, 598 (1979)]. This effect can be reproduced in the real-space theoretical $T(r)$ by convoluting it with a suitable modification function, which is the inverse Fourier transform of the damping function. We used the experimental $Q_{max}=45.2$ and 22.88 $Å^{-1}$ for SiO_2 and sodium silicate glass, respectively.
[69] X. Yuan and A. N. Cormack, J. Non-Cryst. Solids **319**, 31 (2003).
[70] A. C. Wright, A. G. Clare, B. Bachra, R. N. Sinclair, A. C. Hannon, and B. Vessal, Trans. Am. Crystallogr. Assoc. **27**, 239 (1991).
[71] S. N. Houde-Walter, J. M. Inman, A. J. Dent, and G. N. Greaves, J. Phys. Chem. **97**, 9338 (1993).
[72] G. S. Henderson, J. Non-Cryst. Solids **183**, 43 (1995).
[73] A. G. Clare, A. C. Wright, and R. N. Sinclair, J. Non-Cryst. Solids **213-214**, 321 (1997).
[74] I. Farnan, P. J. Grandinetti, J. H. Baltisberger, J. F. Stebbins, U. Werner, M. A. Eastman, and A. Pines, Nature (London) **358**, 31 (1992).
[75] L. F. Gladden, T. A. Carpenter, and S. R. Elliott, Philos. Mag. B **53**, L81 (1986).
[76] R. Dupree, D. Holland, and M. G. Mortuza, J. Non-Cryst. Solids **116**, 148 (1990).
[77] M. J. Duer, S. R. Elliott, and L. F. Gladden, J. Non-Cryst. Solids **189**, 107 (1995).
[78] The smaller simulation box used to prepare the glass used in the CPMD simulations results in different Q^n abundances, which are largely maintained after switching to the CPMD description: therefore the different Q^n distribution in the CPMD run is not related to the CPMD description but only to the system size.
[79] A. N. Cormack and J. Du, J. Non-Cryst. Solids **293**, 283 (2001).
[80] S. K. Lee and J. F. Stebbins, J. Phys. Chem. B **107**, 3141 (2003).
[81] X. Yuan and A. N. Cormack, Comput. Mater. Sci. **24**, 343 (2002).
[82] M.-Z. Huang, L. Ouyang, and W. Y. Ching, Phys. Rev. B **59**, 3540 (1999).
[83] S. Tsuneyuki, M. Tsukada, H. Aoki, and Y. Matsui, Phys. Rev. Lett. **61**, 869 (1988).
[84] M. Benot and W. Kob, Europhys. Lett. **60**, 269 (2002).
[85] S. N. Taraskin and S. R. Elliott, Phys. Rev. B **56**, 8605 (1997).
[86] S.-T. Lin, M. Blanco, and W. A. Goddard III, J. Chem. Phys. **119**, 11792 (2003).
[87] J. Tan, S. Zhao, W. Wang, G. Davies, and X. Mo, Mater. Sci. Eng., B **106**, 295 (2004).
[88] N. Zotov, I. Ebbsjo, D. Timpel, and H. Keppler, Phys. Rev. B **60**, 6383 (1999).
[89] S. Ispas, N. Zotov, S. De Wispelaere, and W. Kob, J. Non-Cryst. Solids **351**, 1144 (2005).
[90] R. G. Hill, J. Mater. Sci. Lett. **15**, 112 (1996).
[91] G. N. Greaves, A. Fontaine, P. Lagarde, D. Raoux, and S. J. Gurman, Nature (London) **293**, 611 (1981).
[92] H. Maekawa, T. Maekawa, K. Kawamura, and T. Yokokawa, J. Non-Cryst. Solids **127**, 53 (1991).